

SHEAR FAILURE OF REINFORCED CONCRETE MEMBERS SUBJECTED TO PRE-CRACKING COUPLED WITH COMBINED AXIAL TENSION AND SHEAR

(Reprinted from Proceedings of JSCE, No.690/V-53, November 2001)



Amorn PIMANMAS



Koichi MAEKAWA

The effect of loading path on the behavior of reinforced concrete (RC) members is investigated. The shear capacity of RC members under pre-cracking coupled with axial tension and shear is discussed. The three main effects of axial tension are (1) early yielding of the main bar due to initial stress; (2) accelerated formation of diagonal cracks, and (3) arrested diagonal crack development as a result of pre-cracks caused by axial tension. The shear capacity may increase or decrease depending on the relative contributions of these three effects. The JSCE design code essentially recognizes the first effect, but has no explicit treatment of the second and the third ones. A comparative study of experimental results, the JSCE code, and FEM predictions is conducted.

Keywords: *pre-cracked RC, non-proportional loading path, failure envelope, path-dependency, coupled axial tension/shear*

Amorn Pimanmas is an assistant professor at the School of Building Facilities and Civil Engineering, Sirindhorn International Institute of Technology, Thammasat University, Thailand. He obtained his Ph.D. from the University of Tokyo in 2000. His research interests relate to nonlinear mechanics and the constitutive laws of reinforced concrete, behavior of damaged reinforced concrete and strengthening of reinforced concrete member. He is a member of the JSCE.

Koichi Maekawa is a professor at The University of Tokyo. He obtained his D. Eng. from the University of Tokyo in 1985. His research interests relate to nonlinear mechanics and the constitutive laws of reinforced concrete and seismic analysis of structures and concrete thermodynamics. He is a member of the JSCE.

1. INTRODUCTION

Reinforced concrete members, whether pre-cracked or initially un-cracked, may be subjected to multi-directional non-proportional load paths (Fig. 1) in the course of their loading history. They may be exposed to volumetric changes induced by drying shrinkage and thermal expansion or contraction under actual environmental conditions. As a result of these loadings, cracks form in the concrete body. These pre-cracks generally have a variety of widths and inclinations. The effect of such pre-cracking on RC behavior has been experimentally investigated by Pimanmas and Maekawa^{1), 2)}. Pimanmas et al.^{2), 3)} have also conducted numerical analysis using FEM to simulate the shear response of pre-cracked RC members^{2), 3)}. The influence of pre-crack width and inclination as well as interactions among neighboring cracks can be satisfactorily simulated. The ability of the fixed smeared crack model employed in FEM to model these effects arises because it reflects the mechanics of pre-cracked elements^{1), 2), 3) 4)}, which are rooted in the shear anisotropy along the pre-crack plane.

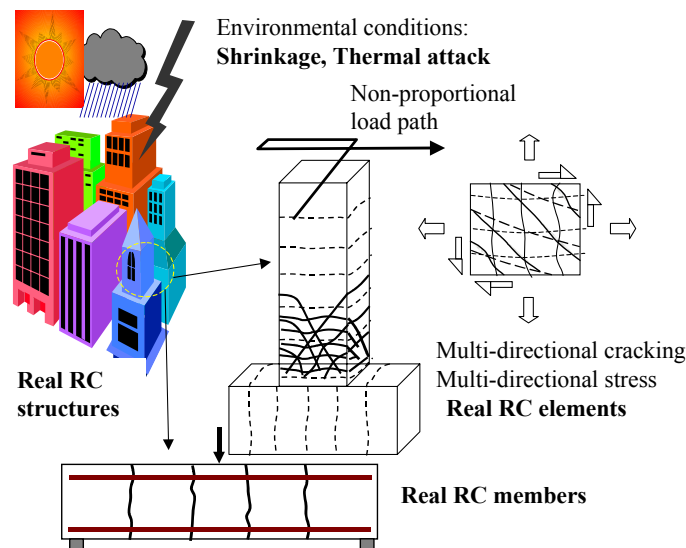


Fig.1 Real RC structures, members, and elements subjected to non-proportional loading paths and real environments

In addition to pre-cracking, the history of loading and environmental attack may concurrently induce pre-stress in RC members. For example, it is known that concrete may be susceptible to drying and autogenous shrinkage as well as thermal deformation at an early age⁵⁾. These mechanisms not only produce cracks but also leave residual or pre-stress in concrete members. Hence, it is necessary to discuss the coupled effect of pre-stress and pre-cracks on RC behavior. Moreover, RC members may be subjected to a non-proportional load path. Concrete is a highly path-dependent material that memorizes past cracking events. Consequently, it is not sufficient to determine the behavior of an RC member from only the start and end points in load space. The entire load path through that the member has experienced must be considered too. Hence, even if two identical reinforced concrete members begin at the same initial load point and reach the coincident end point, their responses may be different if they experience different load paths. In this work, the influence of load path on RC members will be examined by analyzing RC members under combined axial tension-shear with pre-cracking.

2. MECHANICS OF MULTI-CRACKED RC ELEMENT AND SHEAR ANISOTROPY

In order to achieve a numerical simulation to the problem described above, the analytical method must properly reflect the mechanics of a multi-cracked element subjected to a multi-directional stress state. The mechanics of a multi-cracked element are illustrated in Fig. 2. The overall response of a multi-cracked element is the integration of the local responses of all cracks in the element. This assembly of local responses is achieved through enforcement of the compatibility and equilibrium conditions for each crack in the element as well as the un-cracked concrete between the cracks. The behavior of each crack depends on its width and inclination, as well as on the magnitude and direction of applied stresses and interactions with

neighboring cracks. Interaction is the phenomenon by which the loading condition of one crack may cause other cracks to load, unload, or reload depending on their geometrical and physical properties.

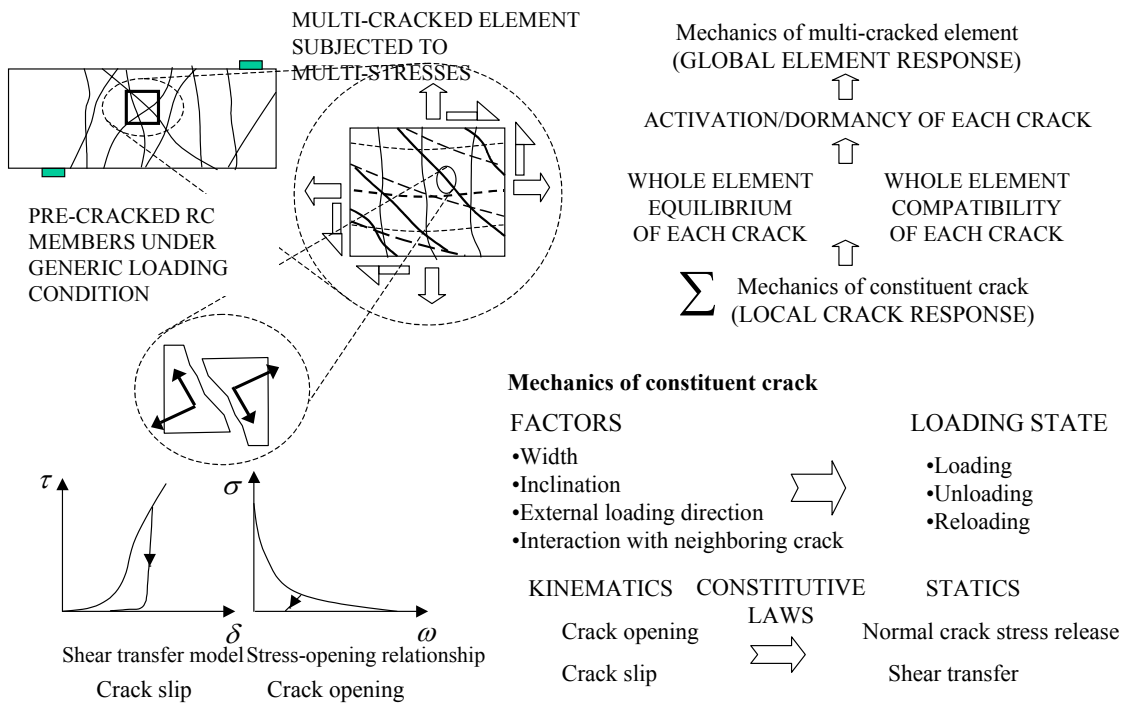


Fig.2 Mechanics of multi-cracked element subjected to multi-stress state

The loading conditions (i.e., the loading, unloading, or reloading) of each crack must satisfy the equilibrium and compatibility conditions in the local crack direction. This local equilibrium and compatibility bring about global equilibrium and compatibility for the RC element. Eventually, the behavior of the entire member is the integration of responses from all elements. Through the simultaneous satisfaction of equilibrium and compatibility conditions for all cracks in an element, certain cracks can be activated while others are idle. This is known as crack interaction, and is a special case of *anisotropy interaction* as shown in Fig. 3. Anisotropy interaction results from the weak shear and normal stress transfer along the cracking plane.

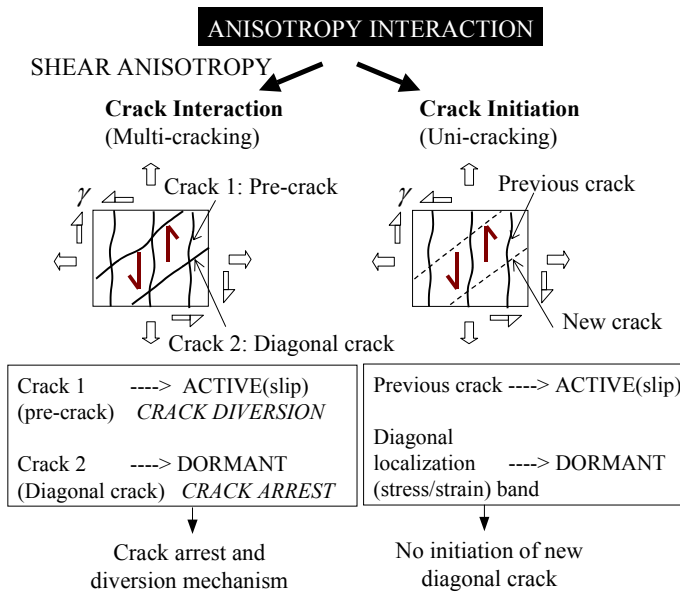


Fig.3 Shear anisotropy and anisotropy interaction

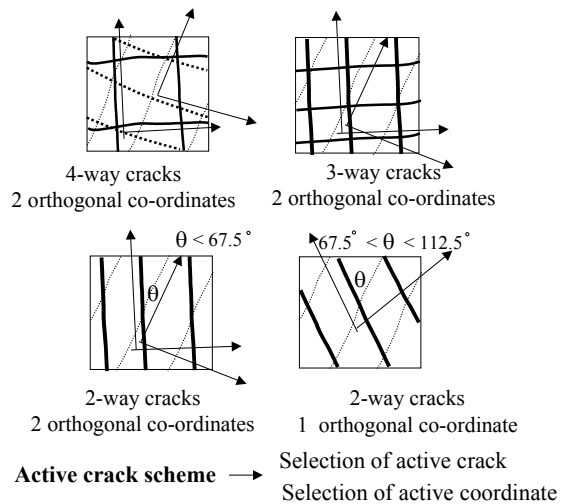


Fig.4 Coverage of four-way fixed crack approach^(6), 7)

An example of anisotropy interaction is explained in more detail in **Fig. 3**. Under the multi-cracking condition (**Fig. 3**, left), some active cracks may dominate overall behavior while other cracks are dormant. Under the uni-cracking condition (**Fig. 3**, right), movement of the active pre-crack relaxes the stress localization in the diagonal direction, which affects the initiation of new cracks. Hence, the activation or dormancy of each crack in the element is governed by anisotropy interaction. In order to simulate shear anisotropy and crack interaction, the smeared RC element in the finite element analysis must be able to capture local crack behavior. Crack kinematics comprise crack opening and slip. The corresponding static variables are normal and shear stresses, respectively, and constitutive laws are required to relate the static to kinematic variables. The constitutive laws include laws for tension stiffening/softening and shear transfer due to aggregate interlock.

3. FOUR-WAY FIXED CRACK MODEL

In order to deal with the situation involving a non-proportional load path and multi-cracking, the fixed crack method and the active crack model are necessary to capture crack interaction. The fixed crack model considers both Mode I tensile stress and Mode II shear stress, thus allowing for the independent and explicit treatment of shear behavior and normal behavior. Consequently, the anisotropy requirement is inherently fulfilled since the principal stress vector does not necessarily coincide with that of principal strain. Moreover, the fixed crack approach records the crack condition and other state variables at all Gauss points, making possible the transfer of path-dependency over the loading path. One recent development related to the fixed crack approach is the four-way fixed crack model proposed by Fukuura and Maekawa^{6, 7}. This crack model can cope with four cracks in distinct orientations at any Gauss point (**Fig. 4**). The applicability of the active crack concept⁸ is extended to the co-ordinate level; that is, concrete stresses are calculated along the active crack in the active co-ordinate. The crack that has the greatest width is considered to be the active one^{6, 7, 8}.

Local constitutive laws are used to compute concrete and reinforcing bar stresses. The coupled tension-compression model, which combines tension stiffening/softening^{8, 9} with the elasto-plastic fracture model⁸, is applied to compute the normal stresses perpendicular and parallel to the crack, respectively. The contact density model¹⁰ is used to compute the shear stress due to aggregate interlock under multi-cracking conditions^{6, 7}. The model for reinforcing bars considers the effect of localized plasticity¹¹ in the vicinity of cracks as well as anisotropic tension stiffening/softening¹². These local constitutive laws have been reformulated and detailed by Fukuura and Maekawa^{6, 7}.

4. ANALYSIS OF PRE-CRACKED BEAM — EFFECT OF PRE-CRACKS

The shear behavior of a pre-cracked beam is investigated analytically and experimentally^{1), 2) 3)}. The experimental program is outlined in **Fig. 5**. Penetrating pre-cracks were introduced into the beam specimen by means of reversed flexural loading (**Fig. 5a**). Two steps of flexural loading were required; after initial flexure, the beam was rotated 180° about its axis and flexure was then applied a second time. To carry out shear testing, supports were moved towards the beam mid-span (**Fig. 5b**) such that the ratio of shear span to effective depth became 2.41. The reinforcement ratio of the main bar was 1.14%. The tested average compressive strength of the concrete was 26.5 MPa. The tested yield strength of the main bar was 338.4 MPa. The process of shear loading caused diagonal crack to propagate across the pre-crack planes.

The dimension and cross section of the beam are shown in **Fig. 6a**. In the analysis, the authors consider two cases: one using smeared elements only and the other using both smeared and discrete joint elements to represent pre-cracks. The finite element meshes of these two cases are shown in **Fig. 6b** and **Fig. 6c**, respectively. These two analyses are referred to as the smeared and smeared-discrete cases, respectively. The load-displacement relationships obtained under shear loading (**Fig. 7**) show that the behavior of the pre-cracked beam significantly differs from that of the non pre-cracked one. The pre-cracked beam reaches considerably greater values of loading capacity, displacement ductility, and energy consumption, but with much lower initial stiffness as compared to the non pre-cracked one.

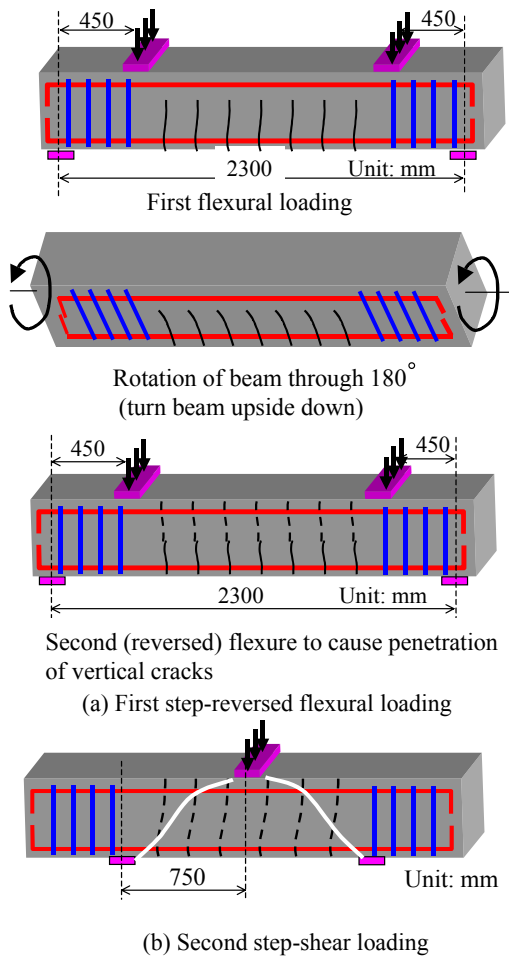
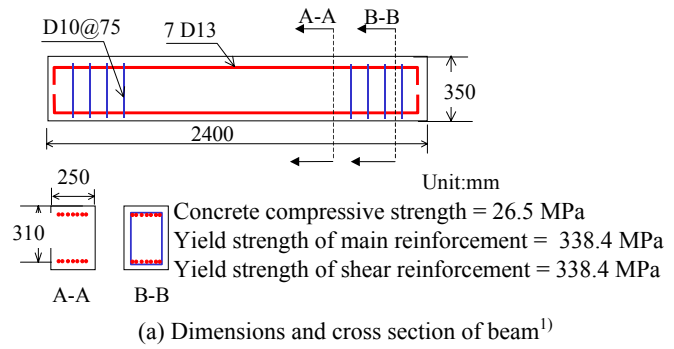


Fig.5 Outline of shear test on pre-cracked beam¹⁾



(a) Dimensions and cross section of beam¹⁾
 Concrete compressive strength = 26.5 MPa
 Yield strength of main reinforcement = 338.4 MPa
 Yield strength of shear reinforcement = 338.4 MPa
 (b) FEM mesh (smearing elements only)
 (c) FEM mesh (smearing + discrete joint elements¹³⁾)

Fig.6 Dimensions, cross section, material properties, and FEM mesh of pre-cracked beam problem

It is noteworthy that the numerical load-displacement curve is not smooth, but jagged like the experimental results. This behavior is ascribed to the crack arrest and diversion mechanism¹⁾. Once a diagonal crack is formed, the load drops. However, the load then continues to increase since the diagonal crack cannot propagate continuously across the pre-crack plane. The full smeared FEM results exhibit some irregularity, since the larger element size adopted is a rough way to model the actual discrete pre-cracks by smeared cracks. The way to more realistically specify the location of pre-cracking is to use smaller smeared elements containing a single crack or joint interface elements. The latter allows for the use of larger sizes of smeared elements to cover the rest of the analysis domain⁸⁾.

Crack patterns obtained during the initial stage for both cases are shown in Fig. 8. Both the smeared and smeared-discrete cases correctly predict the Z-crack¹⁾ around each pre-crack, as seen in the experiment. In pre-cracked beams, Z-cracks are formed as a result of relative deformation between pre-cracks and diagonal cracks¹⁾. The failure crack patterns of the two cases are compared in Fig. 9. FEM suitably models both the main and secondary cracks in both the smeared and smeared-discrete cases. The disconnected pattern of the main failure crack verifies that the analysis is able to simulate the experimental failure mechanism characterized by independent formation of discontinuous diagonal cracks that subsequently combine into the failure crack. There is one point that should be noted regarding the main failure crack path. When smeared elements only are used, the main failure crack is seen as disconnected by the width of one element, as shown in Fig. 9a. However, when discrete joint elements are used, the width of the discontinuity band is greatly reduced (Fig. 9b). Hence, the combined use of smeared and discrete elements seems to give better results⁸⁾.

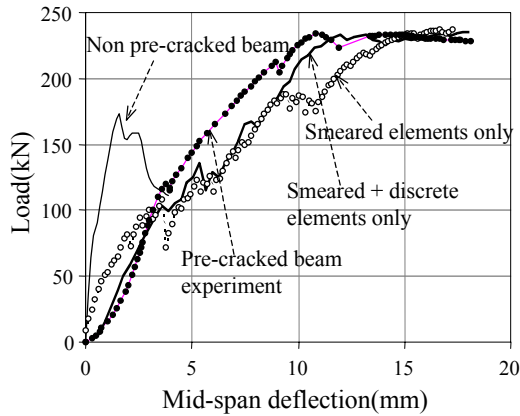
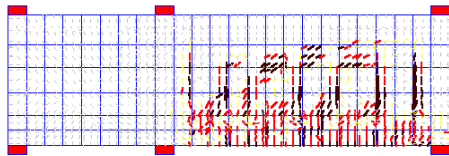
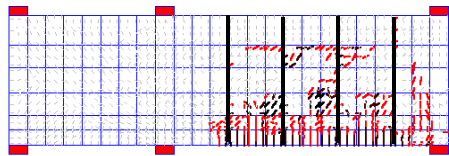


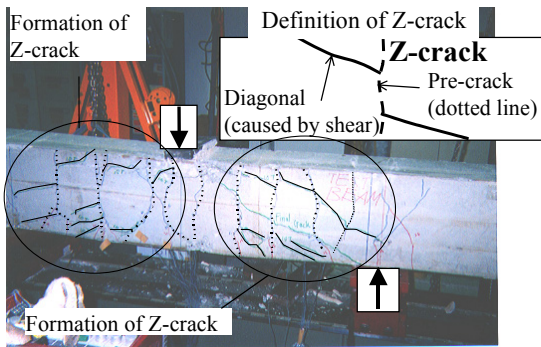
Fig.7 Comparison of numerical and experimental results



(a) Z-cracks predicted in the smeared case

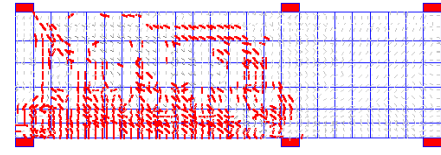


(b) Z-cracks predicted in the smeared-discrete case

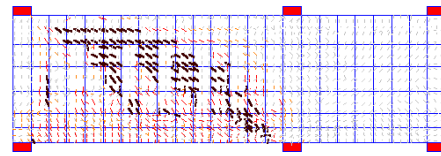


(c) Z-cracks in the experiment¹⁾

Fig.8 Comparison of crack pattern during initial load stage

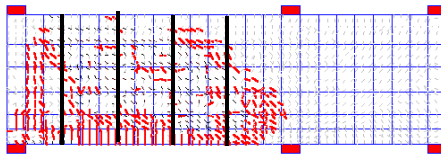


Secondary cracks predicted by FEM

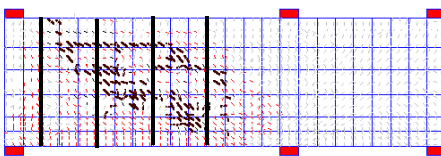


Main failure cracks predicted by FEM

(a) Smeared case

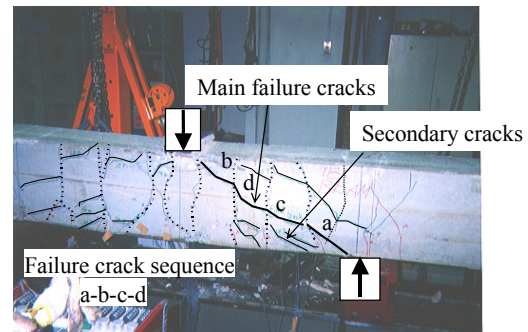


Secondary cracks predicted by FEM



Main failure cracks predicted by FEM

(b) Smeared + discrete case



(c) Experimental failure crack pattern

Fig.9 Comparison of failure crack pattern¹⁾

5. EFFECT OF LOAD PATH ON REINFORCED CONCRETE BEHAVIOR

As noted earlier, the load path is a crucial determinant of RC behavior. Concrete is a highly path-dependent material that retains a memory of past events. The previous loading history and environmental history provide a picture of the initial state of pre-cracking, pre-stress, and pre-strain (that is, the path-dependency) of each RC element constituting the member. Different loading paths, though with the same start and end points, may result in different path-dependencies and hence bring about different structural responses. In this section, the effect of load path on the shear behavior of RC members will be investigated. The problem is defined in Fig. 10. The RC beam is subjected to coupled axial tension and shear loading. In this study, two loading paths are examined. The first is a proportional path in which shear and axial tension are applied simultaneously to the RC beam. Displacement control is used in applying shear, and force control in applying axial tension. In each analysis, the incremental displacement per step is kept constant for shear, while the level of axial tension is varied. Using this loading scheme, it is possible to consider proportional loading paths with various ratios of shear to tension. The second path examined is a non-proportional load

one, with axial tension applied to the beam first, then maintained while shear is superimposed. Two cases are considered: an initially un-cracked RC member and a pre-cracked RC member.

5.1 Coupled axial tension-shear on initially un-cracked RC members and discussion of the JSCE code

The effect of coupled axial tension and shear on initially un-cracked concrete beams is discussed in this section. The finite element mesh and a cross section of the problem are shown in **Fig. 11**. The arrangement is symmetrical, so analysis is carried out on a half beam. No transverse reinforcement is provided in the beam. The beam is designed to fail as a result of unstable propagation of a diagonal shear crack before reinforcement yields. The reinforcement ratio is 1.548%, and the tensile strength of the concrete is 1.62 MPa. The first analysis carried out is for the proportional loading path, and the results are shown in **Fig. 12**. By varying the applied tension in each analysis, the beam achieves different shear capacities.

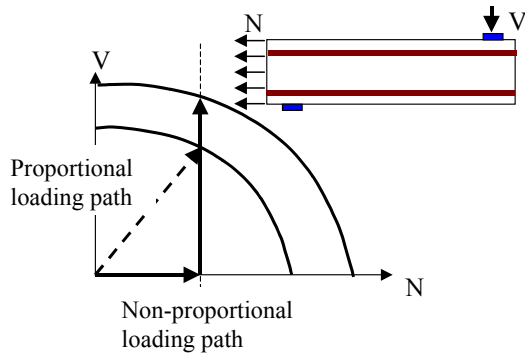


Fig.10 Definition of loading paths in the analysis

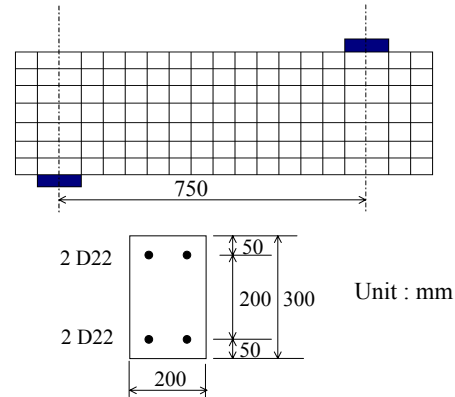


Fig.11 Finite element mesh of the problem

The general tendency is for lower shear capacity to be achieved when the tension applied under proportional loading is higher. This is because the applied tension accelerates formation of the diagonal crack and the first flexural crack, which results in premature appearance of the fall in stiffness. However, the failure process is basically the same as in the beam without axial tension. From the load-displacement relationships obtained under the proportional loading path, we obtain applied tensile stresses at ultimate shear failure as 0.00, 0.39, 0.71, 1.28, 1.84, 2.94, and 3.86 MPa. These tension values will be used in the analysis under the non-proportional loading path.

Analysis for the non-proportional loading path is carried out in two steps. First, pure tension is applied. This is maintained as the initial loading condition, and then shear loading is applied. It should be noted that some of the tensile stresses noted above exceed the tensile strength of the concrete, so vertical cracks may occur. Thus, it is necessary to discuss the coupled effect of pre-cracking and applied tension. The relationship between load and displacement is shown in **Fig. 13**. Two distinct types of behavior can be identified, depending on whether the applied tension exceeds the concrete tensile strength or not. As the level of applied tension increases, a reduction in shear capacity is observed, but the change is not a smooth transition. When the applied tension exceeds the tensile strength, the analysis predicts higher capacity than for lower tensile forces. This indicates that there must be two failure envelopes when the non-proportional loading path is applied. These two modes of behavior are discussed separately below.

First, we discuss the behavior when the applied tensile stress is less than the tensile strength. A typical load-displacement curve has a linearly elastic portion up to a certain point depending on the level of applied tensile stress. As the tensile stress increases, formation of the first flexural crack occurs earlier, causing a noticeable decrease in stiffness. Moreover, the formation of the diagonal crack is also accelerated, which results in premature shear failure. The failure process is basically the same as in the proportional loading case. This type of behavior is exhibited for applied tension levels of 0.39 and 0.71 MPa.

Figure 14 gives a comparison between proportional and non-proportional loading analysis for the case where the applied tension is 0.71 MPa. There is no significant difference between the two cases, except that the shear capacity is slightly lower with the non-proportional loading path. This difference arises because, with the proportional loading path, tension gradually increases from zero. On the other hand, with the non-

proportional loading path, the full tension is applied to the beam from the beginning. A comparison of typical crack patterns between the two cases shows that they are nearly the same, as shown in **Fig. 15**.

Next, the authors discuss the case where the applied tension exceeds the tensile strength of the concrete. In this case, tensile cracks form, resulting in a pre-cracking condition in the beam. As a consequence of these cracks, no elastic portion appears in the load-displacement curve under shear loading. In this case, the effects of crack interaction and pre-tension interfere with each other. Pre-cracking tends to blunt the localization band of the diagonal crack¹⁾, while pre-tension tends to accelerate the early formation of diagonal cracks.

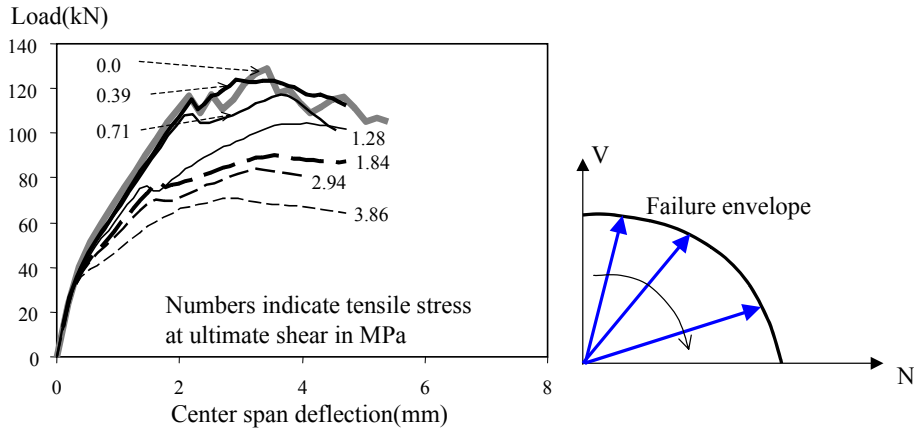


Fig.12 Analytical load-displacement relations under proportional loading path for initially un-cracked RC beam

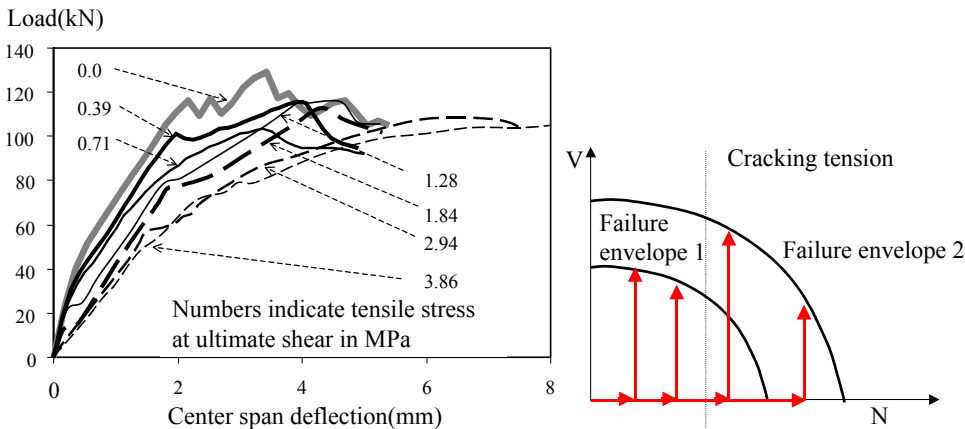


Fig.13 Analytical load-displacement relations under non-proportional loading path for initially un-cracked RC beam

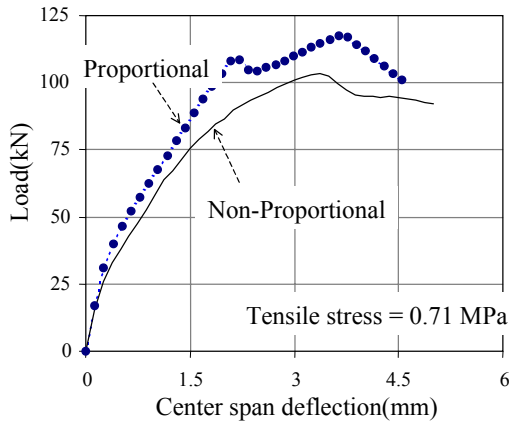


Fig.14 Comparison of proportional and non-proportional loading path analysis for tension = 0.71 MPa

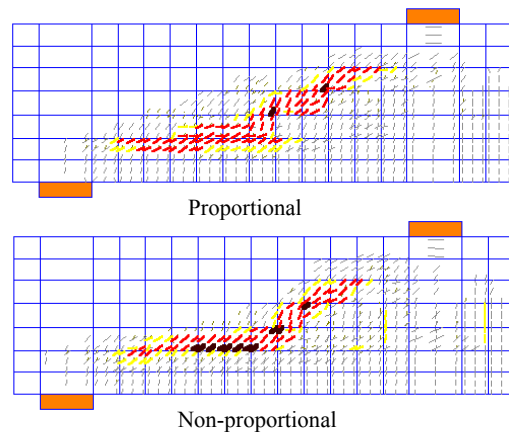


Fig.15 Comparison of crack pattern for proportional and non-proportional loading path (applied tension < tensile strength)

With pre-cracking having this dominant influence, non-proportional loading analysis with an applied tension of 1.84 MPa predicts greater capacity than when the tension is 0.71 MPa (**Fig. 13**). Evidently, if the applied tension exceeds the concrete tensile strength, the effect of vertical cracks also comes into play. The applied tension levels that fall into this category are 1.84, 2.94, and 3.86 MPa. Among these cases, shear capacity falls as the tension increases, which implies that the influence of applied tension outweighs that of pre-cracking. A comparison of load-displacement relationships between the proportional and non-proportional load paths for an applied tension of 3.86 MPa is shown in **Fig. 16**. The beam exhibits much greater shear capacity under the non-proportional loading path, as explained. As for the failure process, **Fig. 17** shows the failure crack pattern for the proportional loading case. Basically, the crack pattern is the same as that in the non pre-cracked beam, except that the diagonal crack is shifted slightly towards the left end of the beam. This diagonal crack, once developed, rapidly propagates in the direction of the loading point and lower support, forming the complete failure path. No crack interaction is exhibited in this case.

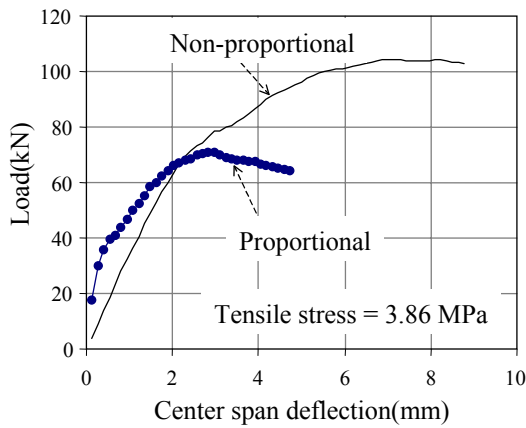


Fig.16 Comparison of proportional and non-proportional loading path analysis for tension = 3.86 MPa

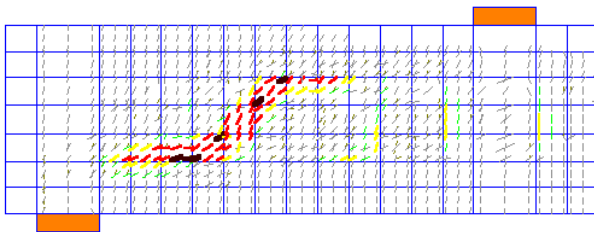
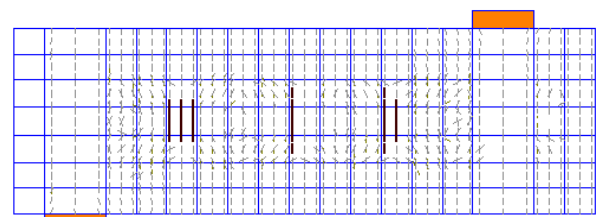
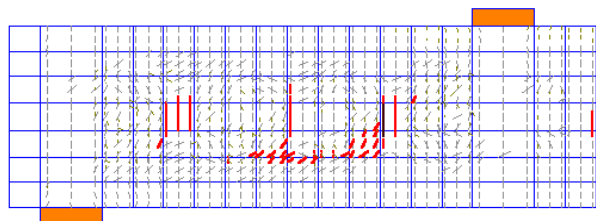


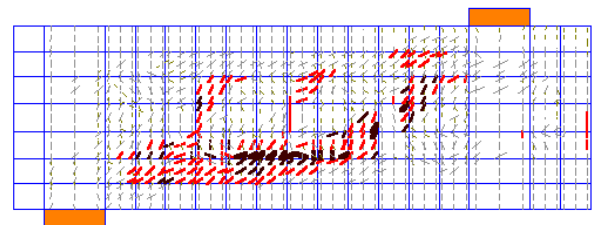
Fig.17 Failure crack pattern for proportional loading analysis, applied tension = 3.86 MPa



(a) Initial crack pattern



(b) Crack arrest phenomenon¹⁾



(c) Z-crack and discontinuity in the diagonal crack propagation

Fig.18 Typical failure crack pattern for non-proportional loading path: applied tension = 3.86 MPa

On the contrary, analysis of the non-proportional loading path results in a different outcome. The initial crack pattern in **Fig. 18a** illustrates the vertical pre-cracks caused by axial tension. Under shear, crack arrest¹⁾ is predicted (**Fig. 18b**). The diagonal crack cannot propagate continuously across the pre-crack planes. Z-cracks are computed as shown in **Fig. 18c**. This demonstrates that crack interaction takes place, and as a result there is greater shear resistance than in the proportional loading case. **Figure 19** gives a comparison of proportional and non-proportional loading results for the case where the applied tension is 1.28 MPa. In the case of the non-proportional loading path, since the applied tension is close to the concrete tensile strength (i.e., $f_t = 1.62$ MPa), the analysis predicts vertical cracking (point *A* in **Fig. 19**) soon after the shear load is applied. **Figures 20** and **21** show the crack patterns under proportional and non-proportional loading for the case where the applied tension is 1.28 MPa. A Z-crack can be distinguished in the crack pattern.

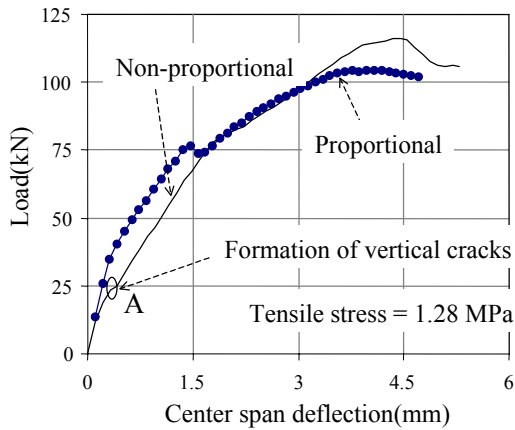


Fig.19 Comparison of proportional and non-proportional loading path analysis for tension = 1.28 MPa

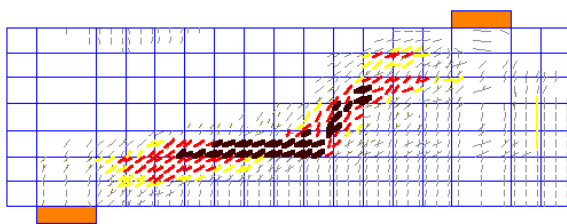


Fig.20 Failure crack pattern for proportional loading path, applied tension = 1.28 MPa

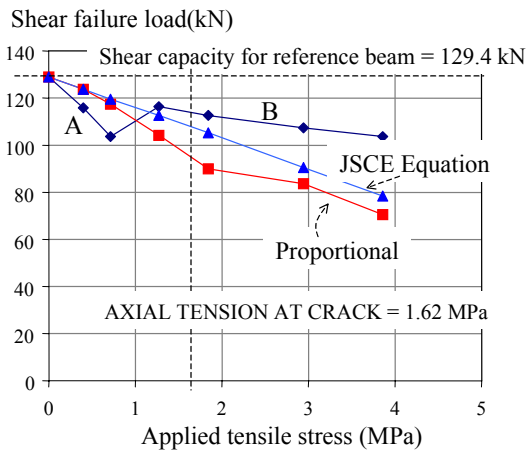
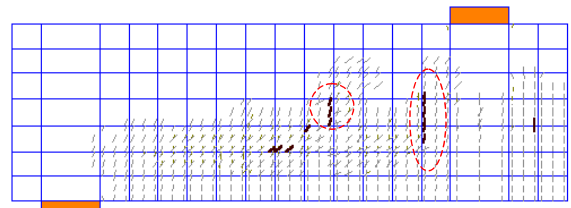
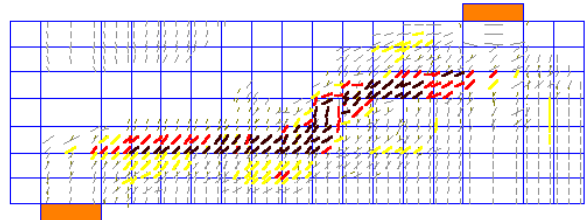


Fig.22 Comparison of failure envelope for proportional and non-proportional loading paths



(a) Formation of vertical cracks corresponding to point A in Fig.19



(b) Failure crack pattern

Fig.21 Typical failure crack pattern for non-proportional loading path: applied tension = 1.28 MPa

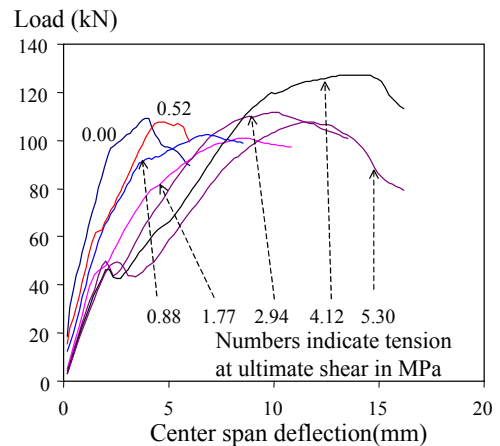


Fig.23 Load-displacement relationship

Figure 22 compares the failure envelopes in the case of proportional and non-proportional loading analysis. With the proportional load path, the failure envelope can be described by a single curve. However, when the loading path is non-proportional, two failure envelopes can be identified. The first, designated curve *A*, represents the case where the imposed axial tensile stress is lower than the tensile strength. Curve *B* represents the case in which the imposed tensile stress is close to or higher than the tensile strength. The gradient of curve *B* is milder than that of curve *A* due to the influence of pre-cracks, which blunt the localization of diagonal crack.

The JSCE design code¹⁴⁾ predicts the reduction in shear capacity of RC members subjected to axial tension by multiplying the basic shear capacity by the factor $\beta_n = 1 + 2M_0/M_u$, where M_0 is the flexural moment counteracting the tensile stress induced by axial force at tensile fiber of the member and M_u is flexural capacity. The JSCE prediction is plotted in **Fig. 22** alongside the analytical failure envelopes. The JSCE

prediction overestimates the envelope in the proportional loading case and in the case of curve *A* for non-proportional loading, but underestimates the FEM results for the non-proportional loading path, curve *B*.

The literature includes some experimental results^{15), 16), 17)} in which no substantial degradation of shear capacity occurs with applied tension. Some investigators¹⁵⁾ have even reported an increase in shear capacity. This confirms that axial tension reduces shear capacity by accelerating diagonal crack formation on one hand, while on the other hand increasing shear capacity by generating pre-cracks which arrest the propagation of diagonal cracks. Generally, shear capacity may be higher or lower depending on the relative contribution made by these two opposing effects. These relative contributions depend on the width of the pre-cracks and the magnitude of the axial tensile stress.

Further analysis is carried out to demonstrate that FEM correctly predicts increases in shear capacity under axial tension. For this purpose, a beam with the same dimensions and cross section as that shown in **Fig. 11** is analyzed again. Here, the reinforcement ratio and tensile strength are assumed to be lower than in the previous case, so as to increase the influence of pre-cracking. The main reinforcement ratio and tensile strength used in this new analysis are 1.2% and 1.18 MPa, respectively.

The results are shown in **Fig. 23**. The failure envelopes predicted by the JSCE design code and this FEM analysis are shown in **Fig. 24**. It is clear that the FEM analysis is able to predict the increase in shear capacity resulting from pre-cracks that blunt the localization of diagonal cracks. The JSCE code takes account of the tensile stress caused in the reinforcing bar by axial tension. In this way, the presence of tensile stress accelerates yielding, hence limiting the maximum load that can be applied to the member. In order to check these results, the FEM analysis is compared with experiments in which specimens failed in shear near or after yielding of the main bars. Two series of shear tests¹⁷⁾ on beam specimens were selected for this purpose. The ratio of shear span to effective depth (*a/d*) is 2.0 and 3.0, respectively, in these tests. The finite element mesh and material properties of these two cases are shown in **Fig. 25**.

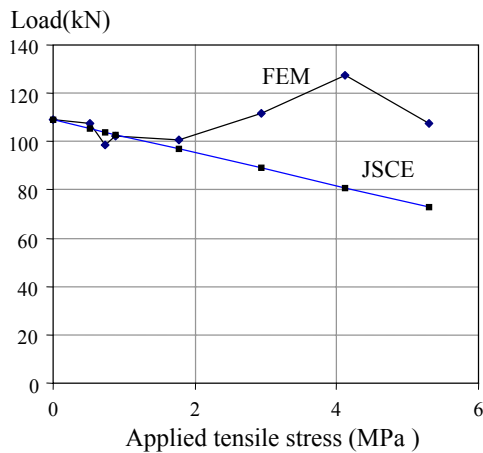
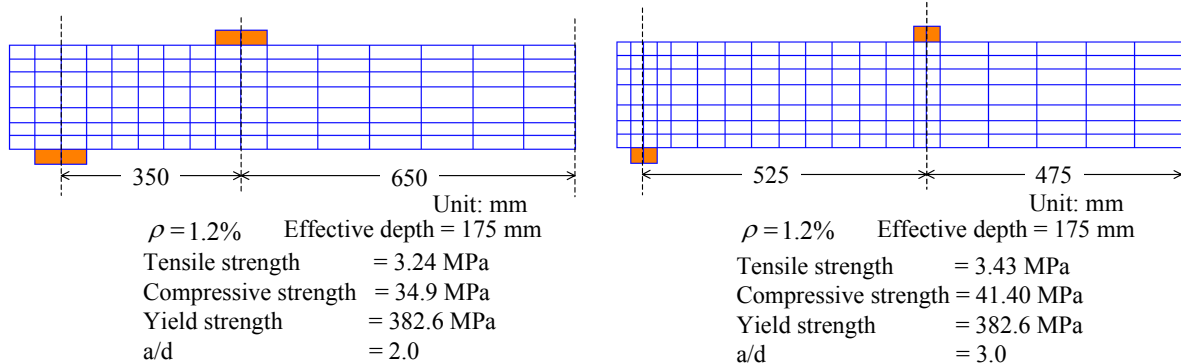


Fig.24 Failure envelope showing dominant influence of pre-cracks

A comparison of the original experimental results with both the FEM and JSCE code predictions is shown in **Fig. 26** and **Fig. 27** for the two *a/d* cases, respectively. The experimental results are modeled reasonably well. The FEM analysis reproduces the experimental trend in which shear capacity falls as the applied tension increases. The failure envelopes demonstrate that FEM closely matches the design code prediction. All three results predict shear failure after yielding. As discussed before, axial tension causes initial tensile stress in the main reinforcement and hence accelerates yielding. Typical numerical failure crack patterns are shown in **Fig. 28** and **Fig. 29** for *a/d* values of 2.0 and 3.0, respectively. The crack patterns indicate both flexural and shear cracking.



(a) Finite element mesh for tested beam with *a/d* = 2.0

(b) Finite element mesh for tested beam with *a/d* = 3.0

Fig.25 Simulation of selected experiment¹⁷⁾

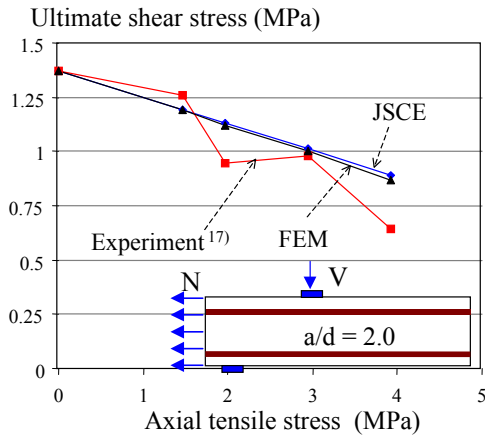


Fig. 26 Comparison of FEM, JSCE, and selected experiment¹⁷⁾ ($a/d = 2.0$)

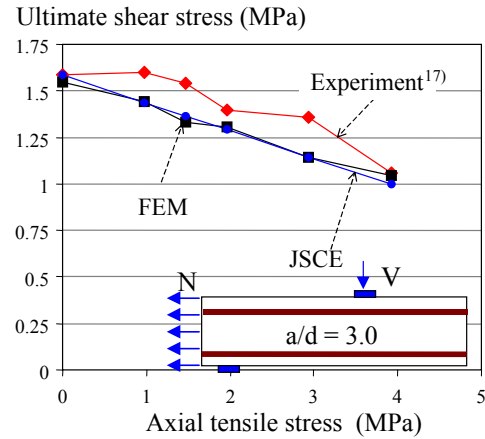


Fig. 27 Comparison of FEM, JSCE, and selected experiment¹⁷⁾ ($a/d = 3.0$)

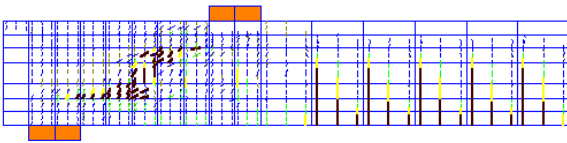
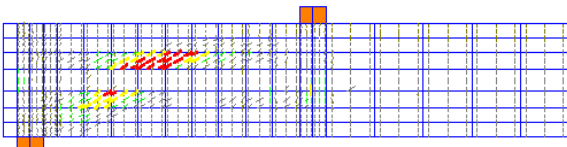
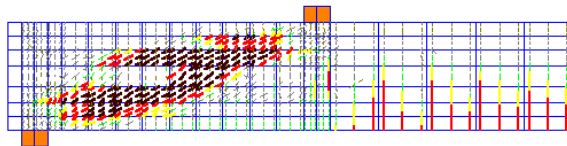


Fig. 28 Numerical crack pattern for $a/d = 2.0$ (tensile stress = 1.96 MPa)



(a) Initial crack pattern: Z-cracks



(b) Failure crack pattern

Fig. 29 Numerical crack pattern for $a/d = 3.0$ (tensile stress = 1.96 MPa)

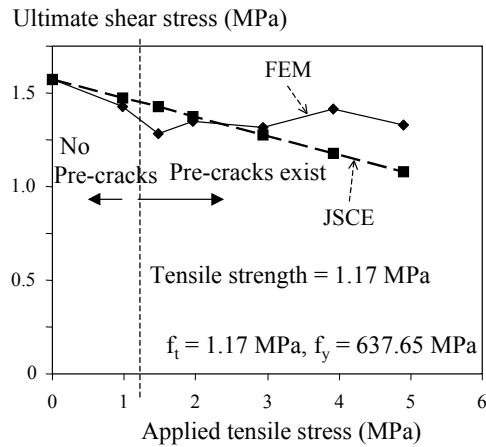
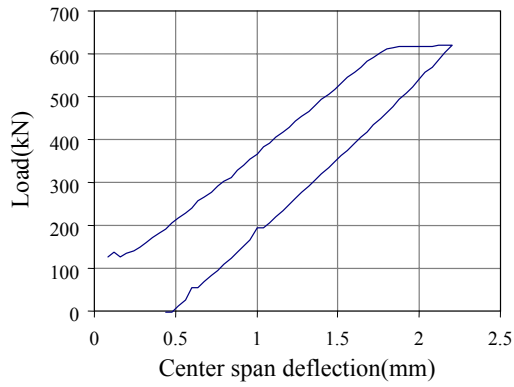


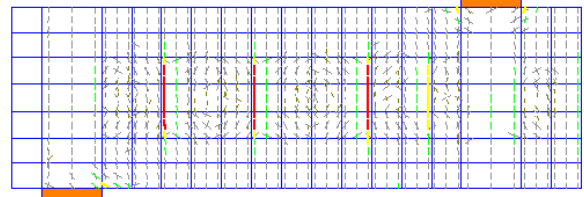
Fig. 30 Failure envelope for beam ($a/d = 3.0$) with dominant influence of pre-cracks

This analysis clarifies that the design code is applicable to problems where shear failure takes place near or after yielding of the main bars. This is because of the effect of initial stress in the reinforcing bars from axial tension, which reduces the yield moment of the beam. Generally, three main effects of axial tension may be identified; that is, (1) initial stress in the reinforcing bars reduces the yielding moment; (2) axial tensile stress tends to accelerate the formation of diagonal cracks; and (3) pre-cracks caused by axial tensile stress tend to inhibit the localization of diagonal cracks. In general, the formula specified in the design code does not take into account the third effect, and consequently provides conservative estimates in practice.

Further analysis is carried out to verify the above understanding. The beam¹⁷⁾ with a shear span to effective depth ratio (a/d) of 3.0 (Fig. 25b) is used once again. However, the yield strength of the main bars is increased to 637.65 MPa, about 1.66 times the actual yield strength in the experiment, in order to force shear failure before yielding of the main bars. Concrete tensile strength is also assumed to be smaller, at $f_t = 1.17$ MPa, compared with the 3.43 MPa in the previous analysis. In this case, the influence of pre-cracking will be dominant. A comparison of the failure envelopes predicted by FEM and by the JSCE formula is shown in Fig. 30. A certain difference between the two predictions can now be seen. In the range of applied axial tensile stress below the tensile strength, the JSCE code specification tends to overestimate shear capacity. However, in contrast, it gives conservative results when the applied tensile stress is higher than the tensile strength.



(a) Load-displacement relationship for axial tension



(b) Initial vertical pre-cracking condition

Fig. 31 Applied axial tension to introduce pre-cracking

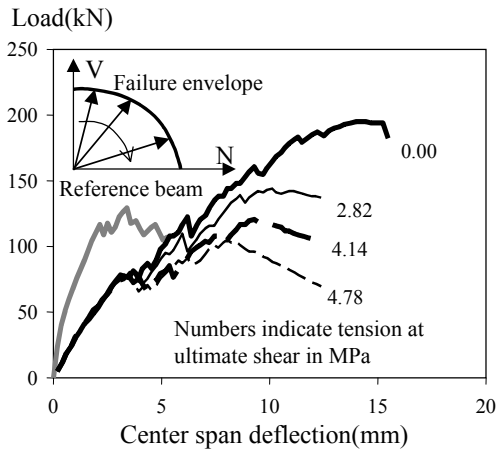
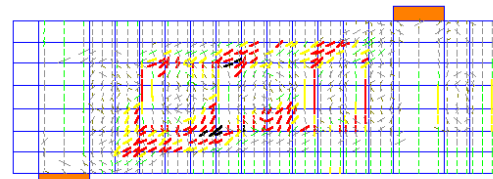
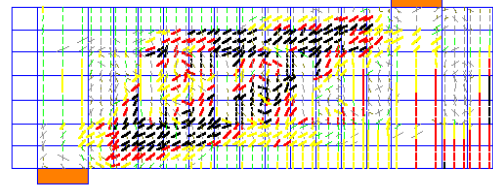


Fig. 32 Analytical load-displacement relations under proportional loading path for initially pre-cracked RC beam



(a) Initial Z-crack pattern



(b) Failure crack pattern

Fig. 33 Crack pattern under proportional loading path, applied tension = 4.78 MPa

5.2 Coupled axial tension-shear on pre-cracked RC members

In the previous section, the main focus of investigations was initially un-cracked RC members. Now, the authors discuss the behavior of initially pre-cracked RC members. The finite element mesh for this analysis is the same as previously used (Fig. 11). The only difference from the previous analysis is the introduction of pre-cracks into the beam. For this purpose, an initial axial tension is applied to the beam to create the pre-cracks. The load-displacement relationship under this initial tension is shown in Fig. 31a. The initial crack pattern is shown in Fig. 31b.

As previously, analysis of the proportional loading path is carried out first. In this case, axial tension is applied simultaneously with the shear load. The load-displacement relationship for each magnitude of applied tension is shown in Fig. 32, demonstrating that shear capacity falls as the applied tension increases. From these load-displacement curves, the magnitudes of applied tensile stress at ultimate shear failure is obtained as 0.00, 2.82, 4.14, and 4.78 MPa. A typical failure process is described in Fig. 33 for the case where the applied tension is 4.78 MPa. The formation of Z-cracks¹⁾ is predicted, as shown in Fig. 33a. The failure crack pattern in Fig. 33b shows the formation of discontinuous diagonal cracks linking the loading point to the support.

Next, analysis of the non-proportional loading path is carried out. First, the above tensile stresses are applied to the beam and kept in place throughout the subsequent shear loading. The load-displacement relationships are shown in Fig. 34. In this case, shear capacity falls continuously as the applied tension increases. Unlike the analysis of initially un-cracked members, the analysis here predicts a single failure envelope. The failure process is basically similar to that under the proportional loading path. The Z-crack and discontinuous diagonal cracks are shown, respectively, in Fig. 35a and Fig. 35b for the case where the applied tension is 4.78 MPa.

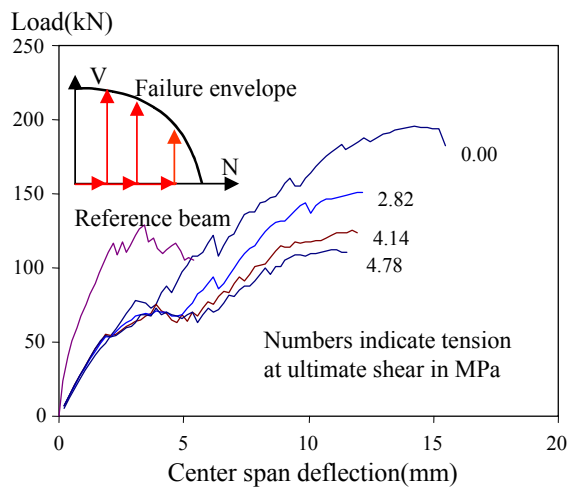


Fig.34 Analytical load-displacement relations under the non-proportional loading path for initially pre-cracked RC beam

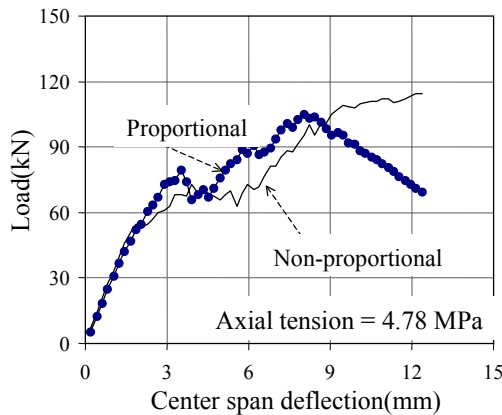


Fig. 36 Comparison of proportional and non-proportional loading path analysis for tension = 4.78 MPa, pre-cracked beam

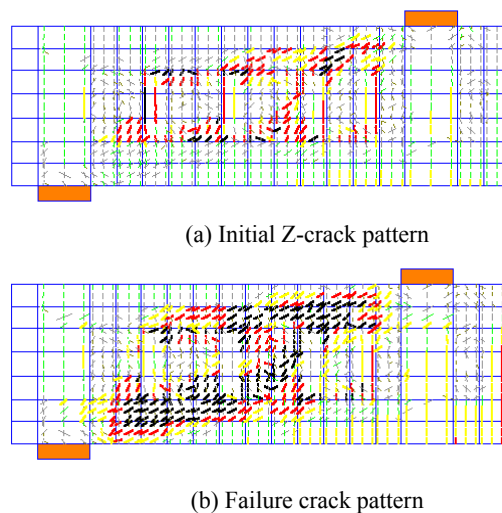


Fig. 35 Crack pattern for the non-proportional loading path, applied tension = 4.78 MPa

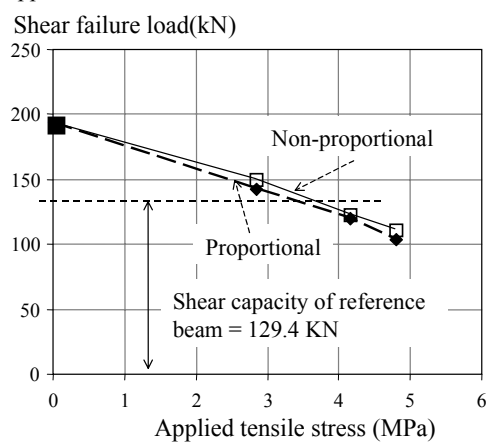


Fig.37 Comparison of failure envelope under proportional and non-proportional loading paths: pre-cracked beam

The load-displacement relationships under proportional and non-proportional loading paths are compared in **Fig. 36** for the case where applied tension is 4.78 MPa. No significant difference can be seen in the curves, though the beam has a slightly higher pre-peak stiffness but slightly lower shear capacity in the case of the proportional loading path. This is because tension gradually increases from zero in the case of the proportional loading path, while it held at a certain value right from the beginning in the case of the non-proportional path. This results in a lower initial tension in the case of the proportional loading path compared with the non-proportional one. At the peak, the applied tensions in the two cases are the same. After the peak, the applied tension in the proportional loading case becomes greater. This explains why the beam exhibits a slightly lower peak capacity when the proportional loading path is followed.

Failure envelopes for the proportional and non-proportional loading paths are shown in **Fig. 37**. Failure envelopes for the initially un-cracked and pre-cracked beams are compared in **Fig. 38**. From these figures, the effects of pre-cracking and pre-tension on shear capacity can be identified. Pre-cracks tend to elevate load capacity while applied tension tends to decrease it. Finally, the authors carry out an analysis of a beam with very large pre-cracks and very high tension. In this case, shear transfer along the pre-cracks is substantially reduced, thus disabling the activation of diagonal cracks. The large pre-cracks are introduced into the beam by applying very high axial tension. The load-displacement relationship under this axial tension and the initial crack pattern are shown in **Fig. 39**. After pre-crack introduction, tensile stresses of 0.49, 2.45, and 4.90 MPa are applied to the beam. Then the shear load is applied. The relationships between load and displacement are shown in **Fig. 40**. The reference beam shown in the figure is one with neither applied tension nor pre-cracking. The results indicate a similar tendency in this case too; that is, shear capacity falls as tension increases.

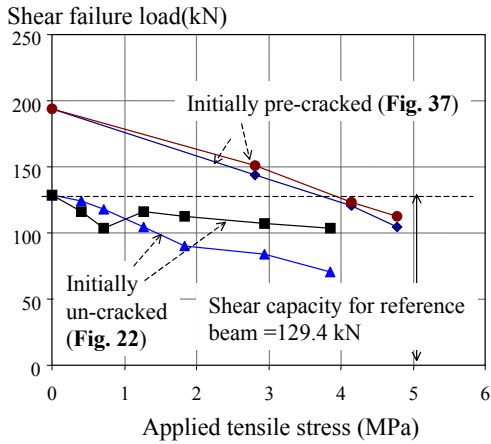


Fig.38 Comparison of failure envelope under proportional and non-proportional loading paths: un-cracked and pre-cracked beam

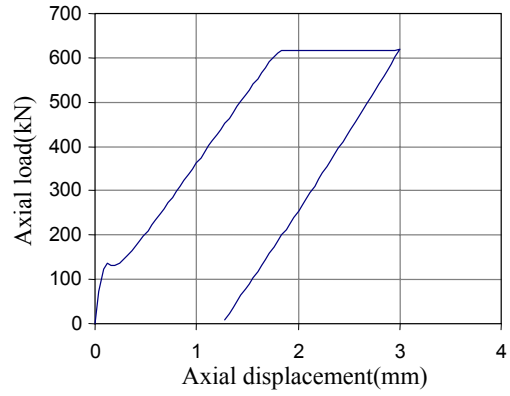


Fig. 39 Applied axial tension to introduce pre-cracking

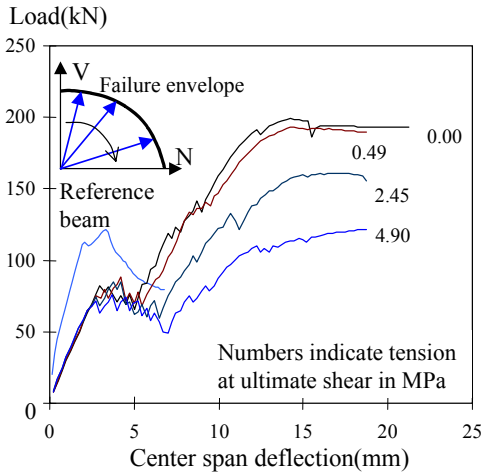
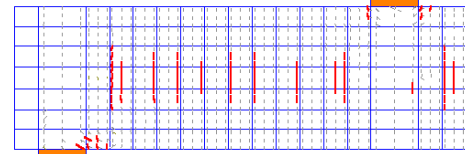
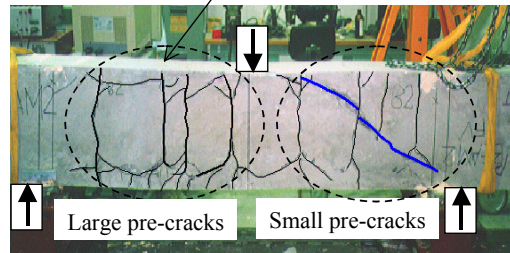


Fig. 40 Analytical load-displacement relations under non-proportional loading path for beams with large pre-cracks



(a) Crack pattern at failure

No diagonal crack in web portion of beam



(b) Experimental crack pattern

Fig. 41 Numerical and experimental crack patterns for very low shear modulus at the pre-crack interface

The crack pattern for the case where the applied tension is 4.9 MPa is shown in **Fig. 41a**. The analysis indicates no diagonal cracking in the web portion of the beam. Instead, the behavior of the beam is governed by pre-tensile stress and pre-cracks rather than diagonal cracks. Since the pre-cracks are very wide, shear transfer due to aggregate interlock is greatly reduced, and so no diagonal cracks are formed in the web portion. This behavior is also seen in experiments, as shown in **Fig. 41b**. Here, the left end of the beam was totally dominated by pre-cracks, and the beam suffered shear failure at the right end, which had comparatively smaller pre-cracks.

6. CONCLUSIONS

This paper addresses RC members subjected to a non-proportional loading path and pre-cracking conditions using numerical analysis. A fixed crack approach is employed since it explicitly and independently treats the normal and shear behavior, which is the key to simulating shear anisotropy at the pre-crack interface. The behavior of an RC member subjected to combined axial tension and shear is investigated. The effect of pre-

stress and pre-cracking is discussed. Depending on the loading path, axial tension has different effects on the shear capacity of the beam.

With a proportional loading path, where shear is applied concurrently with axial tension, the axial tension accelerates formation of the diagonal crack, resulting in premature shear failure. With a non-proportional loading path, where axial tension is applied first and then maintained on the beam while the shear load is applied, axial tension has three main effects: (1) early yielding of the main bar due to initial stress; (2) accelerated formation of diagonal cracks, and (3) arrested diagonal crack development as a result of the pre-cracks caused by axial tension. The second and the third effects counteract each other. Depending on their relative contributions, RC beams subjected to axial tension exhibit various forms of shear behavior, and the shear capacity may be higher or lower with the introduction of tension. The JSCE design code predicts only a reduction in shear capacity in regard to the first effect, without explicit consideration of the second and the third ones.

This work also demonstrates the importance of shear transfer along pre-cracks. The behavior of a pre-cracked beam may be totally dominated by diagonal cracks only, or by pre-cracks only, or by both. This last case is where both pre-crack and diagonal crack deformation have an effect, a situation known as crack interaction or anisotropy interaction. It can be concluded from these results that RC behavior is strongly path dependent. The multi-directional crack model is verified as having more versatility and generality than previously demonstrated.

Acknowledgements

The authors would like to express their gratitude for the receipt of Grant-in-Aid for Scientific Research No. 12450174, which provided financial support for this research.

References

- [1] Pimanmas, A. and Maekawa, K.: Influence of pre-cracks on RC behavior in shear, *J. Materials, Conc. Struct., Pavements, JSCE, 2001*, Vol.50, No.669, pp.227-291.
- [2] Pimanmas, A. and Maekawa, K.: Finite element analysis and behavior of pre-cracked reinforced concrete member in shear, *Magazine of Concrete Research*, Vol.53, No.4, pp.263-282.
- [3] Pimanmas, A. and Maekawa, K.: Multi-directional fixed crack approach for highly anisotropic shear behavior in pre-cracked RC members, *J. Materials, Conc. Struct., Pavements, JSCE, 2001*, Vol.50, No.669, pp.293-307.
- [4] Pimanmas, A., and Maekawa, K.: Control of crack localization and formation of failure path in RC members containing artificial crack device, *J. Materials, Conc. Struct., Pavements, JSCE*, Vol.52, No.683, pp.157-171.
- [5] Mabrouk, R., Ishida, T., and Maekawa, K.: Solidification model of hardening concrete composite for predicting creep and shrinkage of concrete, *Proc. of JCI*, Vol.20, pp.691-696, 1998.
- [6] Fukuura, N., and Maekawa, K.: Re-formulation of spatially averaged RC constitutive model with quasi-orthogonal bi-directional cracking, *Proc. of JSCE*, Vol. 45, pp. 157-176, 1999 (in Japanese).
- [7] Fukuura, N. and Maekawa, K.: Spatially averaged constitutive law for RC in-plane elements with non-orthogonal cracking in up to 4 directions, *Proc. of JSCE*, Vol.45, pp. 177-195, 1999 (in Japanese).
- [8] Okamura, H., and Maekawa, K.: *Nonlinear analysis and constitutive models of reinforced concrete*, Gihodo-Shuppan Co. Tokyo, 1991.
- [9] An, X., Maekawa, K., and Okamura, H.: Numerical simulation of size effect in shear strength of RC beams, *J. Materials, Conc. Struct., Pavements, JSCE*, Vol.35, No. 564, pp.297-316, 1997.
- [10] Li, B., Maekawa, K., and Okamura, H.: Contact density model for stress transfer across cracks in concrete, *J. Faculty of Eng. Univ. of Tokyo (B)*, Vol.40, pp.9-52, 1989.
- [11] Salem, H., and Maekawa, K.: Spatially averaged tensile mechanics for cracked concrete and reinforcement under highly inelastic range, *J. Mater. Conc. Struct., Pavement, JSCE*, pp. 277-293, 1999.
- [12] Hauke, B., and Maekawa, K.: Three-dimensional modeling of reinforced concrete with multi-directional cracking, *J. Materials, Conc. Struct., Pavements, JSCE*, Vol.45, pp.349-368, 1999.
- [13] Mishima, T., and Maekawa, K.: Development of RC discrete crack model under reversed cyclic loads and verification of its applicable range, *Concrete Library of JSCE*, No.20, 1992.

- [14] Standard Specification for Design and Construction of Concrete Structures – 1986 part 1[design], JSCE.
- [15] Yamada, K., and Kiyomiya, O.: Shear resistance of reinforced concrete beams with initial penetrating cracks, *JCI*, Vol.17, No.2, pp. 791-796, 1995 (In Japanese).
- [16] Tamura, T., Shigematsu, T., and Nakashiki, K.: About the increase in shear capacity of RC beams under axial tension, *Proc. of the 54th JSCE Annual Convention*, pp.608-609, 1999 (in Japanese).
- [17] Tamura, T., Shigematsu, T., Hara, S., and Nakano, S.: Experimental analysis of shear strength of reinforced concrete beams subjected to axial tension, *Concrete Research and Technology*, JCI, Vol.2, No.2, 1991.